Arabian Journal of Chemistry (2022) **15**, 103525

King Saud University

Arabian Journal of Chemistry

www.ksu.edu.sa
www.sciencedirect.com

ORIGINAL ARTICLE

Sustainable green synthesis of silver nanoparticles using *Sambucus ebulus* phenolic extract (AgNPs@SEE): Optimization and assessment of photocatalytic degradation of methyl orange and their in vitro antibacterial and anticancer activity

Zahra Hashemi [a], Zirar M. Mizwari [b,c], Sarvin Mohammadi-Aghdam [d], Sobhan Mortazavi-Derazkola [e,*], Mohammad Ali Ebrahimzadeh [a,*]

[a] *Pharmaceutical Sciences Research Center, Hemoglobinopathy Institute and Department of Medicinal Chemistry, School of Pharmacy, Mazandaran University of Medical Sciences, Sari, Iran*
[b] *Department of Medical Laboratory Technology, Shaqlawa Technical College, Erbil Polytechnic University, Erbil, Iraq*
[c] *Rwandz Private Technical Institute, Erbil, Iraq*
[d] *Department of Chemistry, Payame Noor University, P.O. BOX 19395-3697, Tehran, Iran*
[e] *Medical Toxicology and Drug Abuse Research Center (MTDRC), Birjand University of Medical Sciences, Birjand, Iran*

Received 18 August 2021; accepted 26 October 2021
Available online 29 October 2021

KEYWORDS

Biosynthesis;
Silver nanoparticles;
Antibacterial;
Catalytic;
Anticancer;
Sambucus ebulus

Abstract The biogenic approach in the synthesis of nanoparticles provides an efficient alternative to the chemical synthesis system. Furthermore, the ecofriendly synthesis of metallic nanoparticles is developing rapidly due to its wide applications in sciences. In this research, metallic silver nanoparticles (AgNPs) were biosynthesized using *Sambucus ebulus* (*S. ebulus*; AgNPs@*SEE*) extract for the evaluation of efficient antibacterial, anticancer, and photocatalyst activities. The reaction parameters including temperatures, contact time, and $AgNO_3$ concentration were discussed and optimized. The optimized nanoparticles (AgNPs@*SEE*) showed cubic structure, spherical morphology with the average size of 35–50 nm. The photocatalytic performance of AgNPs was assessed by degradation of methyl orange at different concentrations of AgNPs@*SEE* (10 and 15 µl) under sun-light irradiation. About 95.89% of the pollutant was degraded (after 11 min), when 10 µl of nanocatalyst used. Also, the degradation of contaminant increased (about 95.47% after 7 min) by increasing the

* Corresponding authors.
E-mail addresses: S.mortazavi23@yahoo.com, Sobhan.mortazavi@bums.ac.ir (S. Mortazavi-Derazkola), Zadeh20@gmail.com (M. Ali Ebrahimzadeh).

Peer review under responsibility of King Saud University.

Production and hosting by Elsevier

https://doi.org/10.1016/j.arabjc.2021.103525

nanoparticle concentration to 20 µl. All in all, the results showed that the percentage of pollutant degradation increased with increasing the concentration of nanocatalyst. Furthermore, anticancer activity of AgNPs@*SEE* on human cancer cell lines (AGS and MCF-7), and antibacterial activity on both Gram-positive and Gram-negative microorganisms were studied. The synthesized AgNPs@*SEE* exhibited superior performance on cancer cell lines and effective antibacterial properties against Gram-positive microorganisms (like MIC value of 1.5 µg/ml for *S. aureus*) than Gram-negative microorganisms. All these investigations revealed that silver nanoparticles synthesized by natural extract have the potential to use as low-cost and efficient nanoparticles for environmental and biomedical applications.

1. Introduction

Nanoscience is growing rapidly among various areas such as environment, medicine, chemistry, pharmacy, physics, biology, and material science (Mohammadzadeh et al., 2019; Ghoreishi et al., 2017; Mohammadi-Aghdam et al., 2018; Ardestani et al., 2020). The properties of metal nanoparticles are different due to their morphology and size (Ebrahimzadeh et al., 2020). A great deal of investigation have been reported on the synthesis and application of various nanoparticles such as Au (Kumari and Meena, 2020), Ag (Yugay et al., 2020), Pd (Rabiee et al., 2020), ZnO (Yarahmadi et al., 2021), TiO_2 (Pushpamalini et al., 2021), Cu (Mali et al., 2020) etc. Among these nanoparticles, silver nanoparticles have gained attention based on their wide range of applications in medical, catalyst in chemical reactions, nonlinear optics, bio-labeling, and good electrical conductors. Also, pervious researches have shown that metallic AgNPs have high antibacterial activity against various bacteria (Mortazavi-Derazkola et al., 2020; Yousaf et al., 2020; Ebrahimzadeh et al., 2020). To date, different methods such as thermal decomposition, microemulsion/reverse micelles, photochemical, chemical reduction, electrochemical reduction, and radiation assisted have been reported for the synthesis of nanomaterials. Disadvantages of these methods are that they involve hazardous reagents, and solvents which are a serious danger to the environment, humans, and living organisms (Uluturhan and Kucuksezgin, 2007). Moreover, these approaches face numerous problems such as expensive raw materials and instruments, high temperature, and stabilizers. In term of solutions, green synthesis (using the extract) is suggested as a non-toxic, environmentally friendly (without environmental damage method), low-cost process for the fabrication of nanomaterials. Several reports are available on the biosynthesis of noble metal nanoparticles using plant extract like *Azolla caroliniana* (Anjana et al., 2020), *Garcinia indica* (Sangaonkar and Pawar, 2018), *Camellia sinensis* (Rolim et al., 2019), *Spatoglossum asperum* (Ravichandran et al., 2018), *Parkia speciosa* (Ravichandran et al., 2019). *Sambucus ebulus* (*S. ebulus*) is a native perennial herb of the Adoxaceae family. This plant is mainly distributed in Southwest Asia such as the Islamic Republic of Iran, southern and central Europe, and northwest Africa (Shokrzadeh and Saeedi Saravi, 2010). Roots and leaves of this plant are applied in treating sore-throat, and bee bites. Furthermore, *Sambucus ebulus* has been reported to be anti-hemorrhoids, anti-helicobacter pylori, and very useful in the treatment of rheumatism and eczema (Ebrahimzadeh et al., 2006).

Phenolic pollutants are some of the most common organic pollutants presents in different industries such as paper printing, rubber, pharmaceutical, petrochemical, textile, etc. (Gutés et al., 2005; Notsu and Tatsuma, 2004). Photocatalytic degradation experiment is one of the significant routes that have been performed for contaminants degradation from wastewater. This technique shows the potential impact on the widespread spectrum of dye mineralization. In recent years, biogenic nanoparticles have gained more attention for photocatalytic degradation of organic pollutants owing to their unique properties. Recently, various natural agents were used for the synthesis of nanomaterials which revealed promising biological and catalytic activities (Table 1).

In this study, for the first time, we used *Sambucus ebulus* extract as reducing, capping, and stabilizing agents for the fabrication of metallic silver nanoparticle. The synthesized product was optimized and characterized with various analyses. The antibacterial properties of biogenic product were determined against seven ATCC microorganisms and various multi drug-resistant bacteria isolated from a clinical specimen. Furthermore, we have studied the anticancer activity of biosynthesized AgNPs@*SEE* against cancer cell lines (AGS and MCF-7). Finally, the photocatalytic performance of metallic silver nanoparticles was investigated by decomposition of methyl orange under sun-light irradiation.

2. Experimental

2.1. Materials

Silver nitrate ($AgNO_3$), sodium hydroxide (NaOH), and methanol (CH_3OH) solution were purchased from Sigma Company. Double-distilled deionized water was applied throughout the reactions. Mueller Hinton agar and Mueller Hinton broth were purchased from Pronadisa and QUALAB, respectively. Seven bacterial strains such as *K. pneumonia* ATCC 700603, *P. aeruginosa* ATCC 27853, *E. coli* ATCC 25922, *A. baumannii* ATCC 19606, *P. mirabilis* ATCC 25,933 (Gram-negative) and *E. faecalis* ATCC 29212, *S. aureus* ATCC 29,213 (Gram-positive) were procured from Microbial collection of Iran selected. Antibacterial property of obtained AgNPs@*SEE* was observed against multi-drug resistant clinical isolates were obtained from medical hospitals of Sari, Iran.

Table 1 The nanoparticles prepared from various plants by different researchers.

Sample no.	Plant	Part	Product	Application	References
1	*Coriander sativum*	Leaf	Ag	Antibacterial, antioxidant and anticancer activities	(Alsubki et al., 2021)
2	*Boletus edulis*	Fruit	Ag	Antibacterial, antifungal and anticancer activities	(Kaplan et al., 2021)
3	*Mentha aquatica*	Leaf	Ag	Catalytic and antibacterial activities	(Nouri et al., 2020)
4	*Trigonella foenum-graecum*	Seed	Ag	Catalytic and antibacterial activities	(Awad et al., 2021)
5	*Terminalia bellirica*	Fruit	Ag	Catalytic and antibacterial activities	(Sharma, 2021)
6	*Azolla caroliniana*	Leaf	Ag	Cytotoxicity, catalytic and antibacterial activities	(Anjana et al., 2020)
7	*Solanum trilobatum*	Leaf	NiO	Catalytic and antibacterial activities	(Ezhilarasi et al., 2020)
8	*Citrus sinensis*	Fruit	Ag	Antibacterial, antifungal and catalytic activities	(Anwar and Alghamdi, 2020)
9	*Actinidia deliciosa*	Peel	SnO_2	Catalytic activity	(Gomathi et al., 2021)

Table 2 Preparation conditions of samples.

Sample	$AgNO_3$ Concentration (mM)	Temperature (℃)	Time (h)	Figure of UV
1	1	45	2	Fig. 1a
2	5	45	2	Fig. 1a
3	10	45	2	Fig. 1a
4	15	45	2	Fig. 1a
5	20	45	2	Fig. 1a
6	20	Room temp.	2	Fig. 1b
7	20	60	2	Fig. 1b
8	20	85	2	Fig. 1b
9	20	85	0.75	Fig. 1c
10	20	85	4	Fig. 1c
11	20	85	6	Fig. 1c

2.2. Preparation of Sambucus ebulus extract

The *S. ebulus* were obtained from the Mazandaran province of Iran. The parts of plant were dried at room ambient, and then powdered. Next, 150 g of dried powder was extracted with methanol solution by percolation process (Shirzadi-Ahodashti et al., 2021). After filtering the extract, methanol solvent was removed using a rotary vacuum evaporator (Hei zbad WB eoc, Germany). Finally, about 10 g of extract was achieved, which was used during the synthesis of nanoparticles.

2.3. Green synthesis of silver nanoparticles using S. Ebulus extract (AgNPs@SEE)

The *S. ebulus* extract capped AgNPs (AgNPs@*SEE*) was prepared using our previous protocol (Naghizadeh et al., 2021) with slight modification. Silver nanoparticles (AgNPs) were synthesized by reducing the silver nitrate ($AgNO_3$) with *S. ebulus* extract. To this end, 12.5 ml of filtrate of *S. ebulus* extract (the pH of the solution was adjusted to 10–11) was dissolved in deionized water and added to the aqueous solution of $AgNO_3$ (25 ml; 20 mM) under vigorous stirring for 2 h. After 2 h, the light yellow colored mixture changed to dark brown, an evidence for the preparation of silver nanoparticles ($Ag^+ \rightarrow Ag^0$). The reduced mixture was purified by repeated centrifugation for 5 min, and the obtained precipitate was dried in the oven for 24 h. The effect of various physicochemical conditions (temperature, concentration of silver nitrate, and contact time) on the synthesis of AgNPs was studied to obtain the optimum values (Table. 2).

2.4. High-Pressure liquid chromatography (HPLC)

The HPLC analysis was performed by following the procedure as reported elsewhere (Shirzadi-Ahodashti et al., 2021; Shirzadi-Ahodashti et al., 2020). UV–Vis spectrophotometric detector and solvent delivery system equipped with a Rheodyne injection valve was applied for the HPLC system. A mobile phase consists of a gradient solvent system with methanol and H_2O with 9% glacial acetic acid, which was named solvent A and solvent B in conditions: 5% solvent A from 0 to 5 min and kept at 10% solvent A from 5 to 15 min, 30% solvent A from 15 to 27 min and 80% solvent A from 27 to 45 min were used to elute the sample via an ODS-C18 column (Shim-pack VP-ODS: 250 mm × 4.6 mm id, 5 mm). The flow rate was set at 1 ml/min, and all the measurements were carried out at room ambient. Moreover, the UV–Vis detector (275 nm) was used for detection. The phenol and flavonoid content in the *S. ebulus* extract were analyzed via the current system.

2.5. Multi-drug resistant bacteria from clinical isolates and ATCC strain

Antibacterial activity of green synthesized silver nanoparticles using *S. ebulus* extract (sample no. 10) was carried out against multi-drug resistant (MDR) bacteria, including: *S. aureus*, *A.*

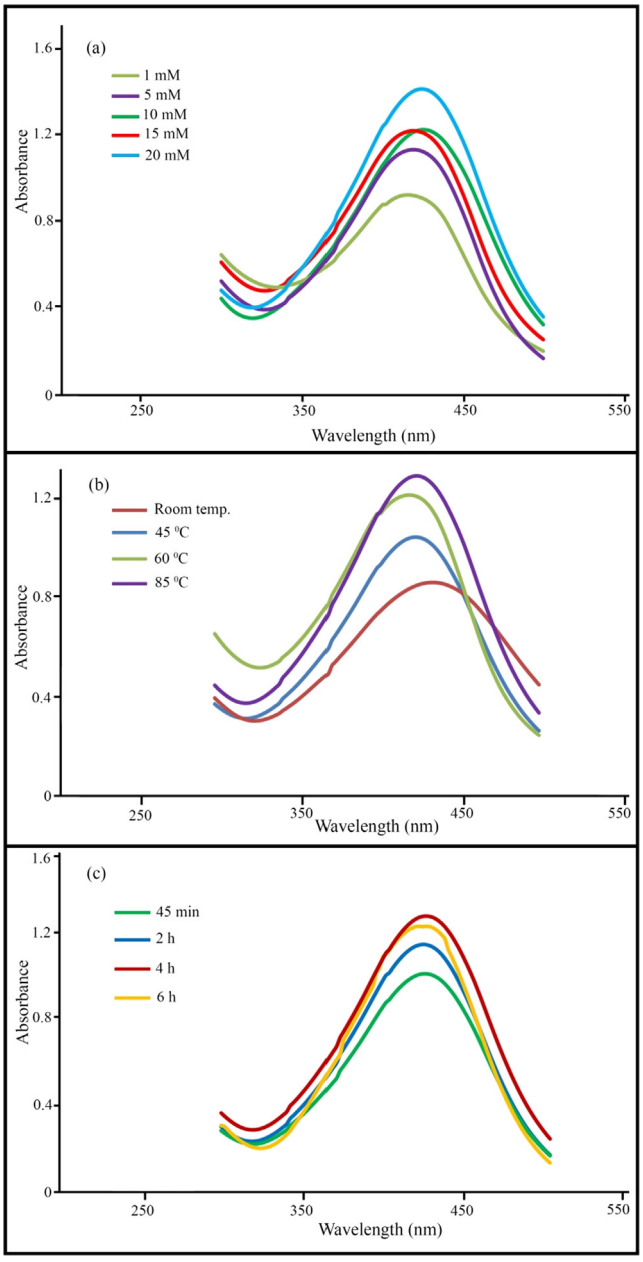

Fig. 1 UV–Vis spectra of the synthesized AgNPs@*SEE* for optimization at various (a) $AgNO_3$ concentrations, (b) temperature and (c) time.

baumannii, *P. mirabilis*, *E. faecalis*, *E. coli*, *K. pneumonia,* and *P. aeruginosa*. The sources of the clinical isolates were blood peripheral, urine, chip, wound, and phlegm. Each isolated bacteria was purified and identified by standard microbiological methods which they were resistance against several antibiotic. Moreover, seven strain bacteria (*P. aeruginosa*, *E. faecalis*, *E. coli*, *S. aureus*, *P. mirabilis*, *A.baumannii* and *K. pneumonia*) were applied to evaluate the antibacterial property of AgNPS (sample no. 10) and compared with ciprofloxacin as a conventional antibiotic. The micro-dilution method was applied to evaluate the minimum inhibitory concentration (MIC) of biosynthesized AgNPs. In this experiment, positive control (antibiotic ciprofloxacin) and negative control (water and extract) were used. 100 µl of Mueller-Hinton broth (MHB) containing various concentrations of silver were added to all wells at 25 ℃. Afterward, 100 µl of dilute bacterial suspension was added to each well and the plates were incubated at 37 ℃ According to MIC value, the minimum bactericidal concentration (MBC) was determined using Muller Hinton agar media at separate plates. Several MIC dilutions were cultured for 24 h at 37 °C. After 24 of growth, the MBC value was measured as the lowest concentration of the tested agent, which showed no visible growth on the plates (Celiktas et al., 2007).

2.6. In-vitro cytotoxicity studies

Cytotoxicity was determined by adopting the procedures as described previously (Ebrahimzadeh et al., 2021). Human gastric cancer (AGS), human breast adenocarcinoma (MCF-7), and human normal fibroblast foreskin (HFF) cells were prepared from pasture Institute, Iran. The cytotoxicity effect of the synthesized AgNPs@*SEE* on two cancer cell lines and one normal cell line was performed by dimethyl thiazolyl tetrazolium bromide (MTT) assay. The cells were grown in RPMI-1640 containing FBS (10%). All cell-cultured media were enriched by FBS (10%), and penicillin/ streptomycin cells in monolayer ($6–10 \times 10^{-3}$) were plated in 96-well plates and incubated for 24 h under CO_2 at 37 °C. After 24 h, cultured cell supernatant was removed and various concentrations of AgNPs@*SEE* (were added to culture medium supplemented (FCS 10% and antibiotics). The cancer cells and control culture medium were treated with different concentrations of AgNPs (10 to 240 µg/ml) and dimethyl sulfoxide (DMSO), respectively. Next, the plates were incubated for 24 h, and 20 µl of MTT (5 mg/ml) was added to each well and incubated for 4 h. Finally, purple color formazan crystals formed were dissolved in DMSO solution (200 µl). The optical density of each well was measured with a spectrophotometer (Biotek Instruments; USA) at 590 nm. The % cell viability was evaluated using the following formula: Percentage of cell viability = (A_{590} nm of treated cells/A_{590} of control cells) × 100 (1)

2.7. Photocatalytic degradation of methyl orange (MO)

The photocatalytic performance of green synthesized AgNPs@*SEE* was studied via the degradation of methyl orange (MO) as a dye contaminant in the presence of $NaBH_4$. 2 ml of deionized water and 50 µl of 5 mM pollutant solution were added to 100 µl of fresh 0.1 M $NaBH_4$. In this research the concentration of silver nanoparticles was 0.8 mg ml^{-1} (8 mg of nanoparticles in 10 ml deionized water). Then, 10 and 15 µl of green synthesized AgNPs were added to the mixture. This process was monitored by UV–Vis spectra at various times. The kinetics of reaction can be explained as in $(A_t/A_0) = -kt$ (2); where t is the reaction time and k is the apparent first-order rate constant (min^{-1}). A_t and A_0 are investigated as the absorption of pollutant at times t and 0, respectively.

3. Results and discussions

3.1. UV–visible spectroscopy

The green synthesis of metallic silver nanoparticles was monitored with color change and UV–Vis spectroscopy (U-2900

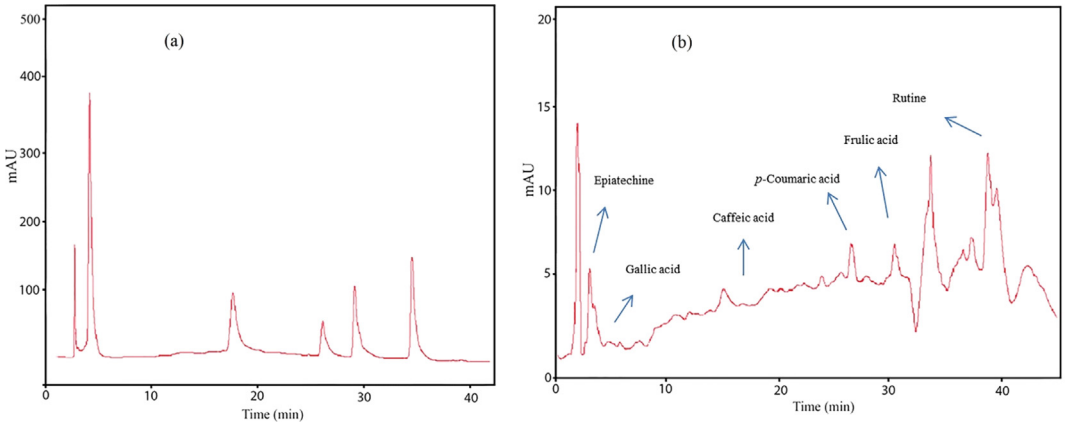

Fig. 2 HPLC profiles of *S. ebulus* extract analyzed at 275 nm. (a) *Standards*, (b) *S. ebulus* extract.

Table 3 Phenolic acid content in *S. ebulus* extract.

Phenolic acid	Retention time (min)	*Sambucus ebulus*
Epiatechine	2.87	4.3
Gallic acid	4.3	1.5
Caffeic acid	17.5	8.4
p-Coumaric acid	26.5	11.1
Frulic acid	29.9	1.8
Rutin	35.4	13.6

Hitachi spectrophotometer) due to the excitation of the surface plasmon resonance (SPR). Various parameters such as temperature, concentration of silver nitrate, and reaction time had significantly effect on shape and size of AgNPs and the UV–Vis spectrum showed the critical role of these parameters for the formation of metallic silver nanoparticles. The absorption spectra of the silver nanoparticle synthesized using *S. ebulus* extract are shown in Fig. 1. By increasing the $AgNO_3$ concentration, color of the AgNPs@*SEE* changed from light yellow to brown and then to dark brown. The $AgNO_3$ (Ag^+) was reduced to silver nanoparticles (Ag^0) in presence of reducing polyphenols and flavonoids in *S. ebulus* extract. Fig. 1a shows the UV–Vis spectra of AgNPs was determined at various concentrations from 1 to 20 mM. As can be seen (Fig. 1a), the plasmon absorbance increased with the increasing concentration of silver nitrate. SPR band shifted from 438 to 432 nm (blue shift) by varying the silver ion concentration from 1 to 20 mM. The effect of temperature plays a key role in the synthesis of AgNPs which can be seen from the UV spectra of the AgNPs synthesized at room temperature, 45, 60, and 85 °C (Fig. 1b). The UV/Vis spectra revealed that by increasing the reaction temperature, the intensity of the absorption peak increased. These differences in SPR peaks may have occurred due to some change in the morphology or size of products (Pereira et al., 2020). In total, the temperature selected in our study was 85 ℃ as shown in Fig. 1b. Fig. 1c reveals the UV–Vis absorption spectra of the mixture of silver nitrate and *S. ebulus* extract as a function of time (0.75, 2, 4, and 6 h). The UV–Vis spectrum indicated a sharp decrease in the absorption after 4 h which indicating the AgNPs synthesis reaction tended towards aggregation. Therefore, the best contact time for the reduction of silver ions was obtained after 4 h.

3.2. HPLC analysis

The HPLC method was applied for the simultaneous determination of phenolic acids in a *S. ebulus* extract. Fig. 2 illustrated the chromatograms of the *S. ebulus* extract and the standards. In this experiment, it was clear that a binary gradient solvent system could be used to separate of phenolic acids and flavonoids in *S. ebulus* extract. HPLC analysis showed that the main compounds in the water extracts are phenolic acid and flavonoid compounds, including: caffeic acid, catechin, rutin, p-coumaric acid, frolic acid and gallic acid (Table. 3). The suggested mechanism for the formation of silvered nanoparticles in presence of *S. ebulus* extract is presence of Fig. 3. According to the HPLC results, rutin (13.6 μg ml^{-1}) was the main antioxidant among the other standards. In general, the mechanism of AgNPs synthesis in presence of a flavonoid is related to the *ortho*-hydroxyl groups. Reduction of Ag^+ into Ag^0 stimulates by releasing two electrons in the flavonoid ring. The flavonoid is finally oxidized into 3′,4′-quinone ring as a stable final product. As the reaction proceeds, Ag undergoes further aggregation to larger clusters and finally forms AgNPs. The quinone form of rutin is also attached to the surface of nanoparticles which leads to less aggregation of Ag^0 in nano size.

3.3. Morphological studies

The size and morphology of the green synthesized silver nanoparticles using *S. ebulus* extract were analyzed by field emission scanning electron microscopy (TESCAN BRNO-Mira3; FE-SEM). The FE-SEM images of the AgNPs@*SEE* (sample no. 10) were presented in Fig. 4. The image obtained by the FE-SEM showed spherical morphology of silver nanoparticles from extract of *S. ebulus* used as reducing and capping agents. In this study, particles size of the AgNPs was determined 40–60 nm. TEM analysis was used to determine particle size distributions and morphological characteristics of AgNPs@*SEE* (sample no. 10). Transmission electron microscopy (Zeiss-EM10C-100 KV; TEM) analysis was used to study the grain structure of synthesized silver nanoparticles in detail. The TEM image (Fig. 5) showed that the morphology of the synthesized AgNPs@*SEE* was spherical and oval with particle size about 35–50 nm. The presence of more than one reducing agent in the *S. ebulus* extract can be one of the rea-

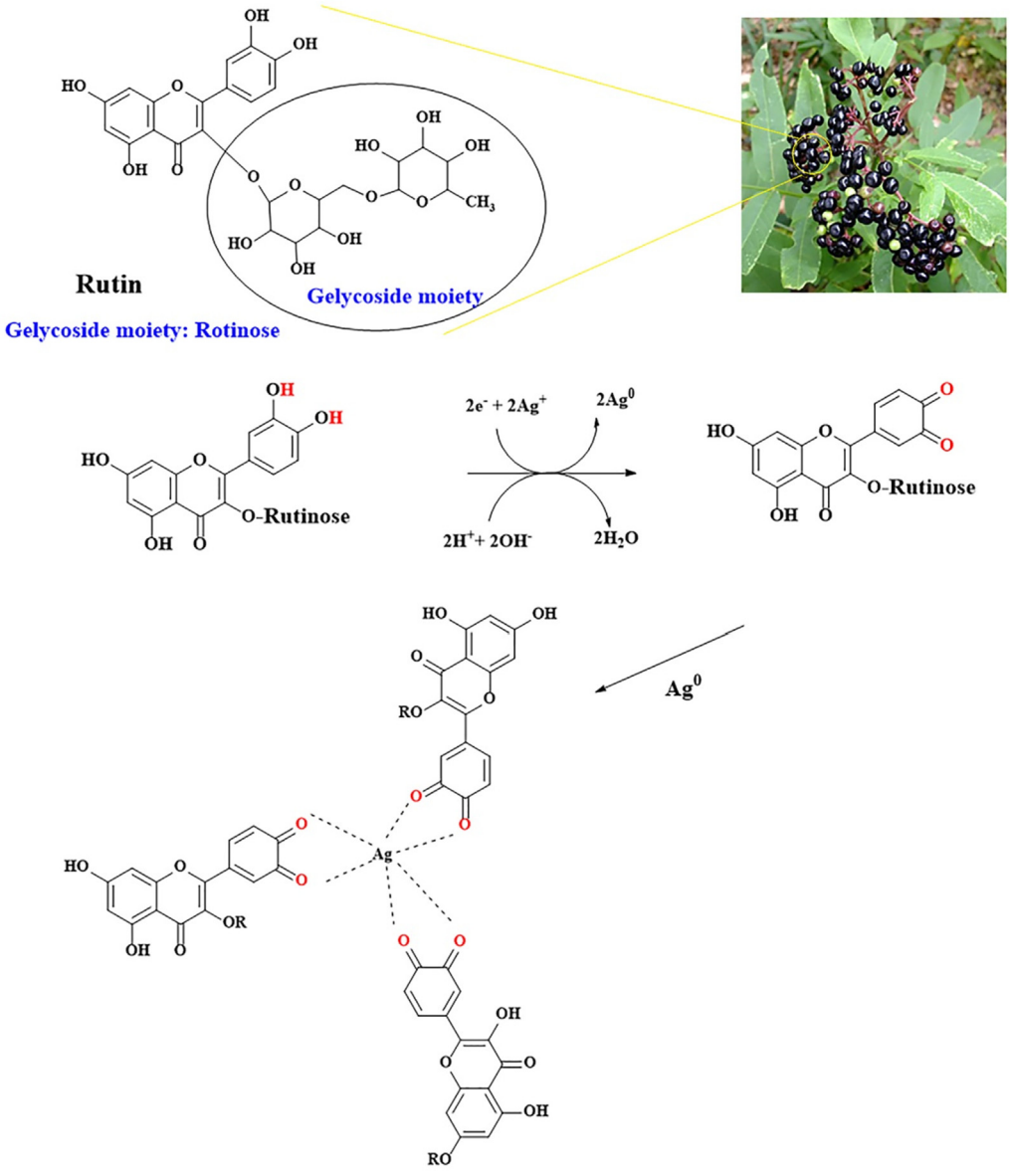

Fig. 3 The possible mechanism of the green synthesized of silver nanoparticles using *S. ebulus* extract.

sons for the formation of different size and shape nanoparticles (Patil and Kim, 2017). The elemental analysis (EDS) recorded from the biosynthesized AgNPs is shown in Fig. 6. The EDS analysis showed an intense silver signal and weak oxygen and carbon peaks. Oxygen (O) and carbon (C) elements are most likely associated with the organic compounds from the *S. ebulus* extract absorbed on the surface of AgNPs@*SEE*, which have a crucial role in reducing and capping agents of AgNPs. Similar AgNPs exhibited strong absorption spectra in the range 2.5–4 keV (Maity et al., 2020).

3.4. X-ray diffraction (XRD)

The crystalline nature of AgNPs@*SEE* was further confirmed by X-ray diffraction pattern (Philips X'pert PRO with Cu-Kα irradiation) (Fig. 7). The XRD pattern demonstrated the FCC (centered cubic face) crystalline structure of AgNPs@*SEE*. Four characteristic diffraction peaks were found at $2\theta = 38.1°$, 44.12°, 64.39°, and 77.11°, which were assigned to the (1 1 1), (2 0 0), (2 2 0), and (3 1 1) planes. Additionally, the mean crystallite size of silver nanoparticles was measured using Scherrer's formula (Oliveira et al., 2019; Shirzadi-Ahodashti et al., 2020): $D = 0.9\lambda/\beta\text{Cos}\theta$ (3); where β full width half maximum, λ the wavelength, D is the size, and θ Bragg's angle. Due to the Scherrer equation, the average particle size of the AgNPs@*SEE* was about 39 nm. Similar XRD peaks were reported from Urtica dioica (Jyoti et al., 2016).

3.5. FT-IR analysis

Fourier-transform infrared spectroscopy (Nicolet Magna-IR 550; FTIR) was carried out to identify the responsible biomolecules of *S. ebulus* extract for stabilization and reduction of AgNPs@*SEE* (sample no. 10). Fig. 8 shows the FT-IR spectra

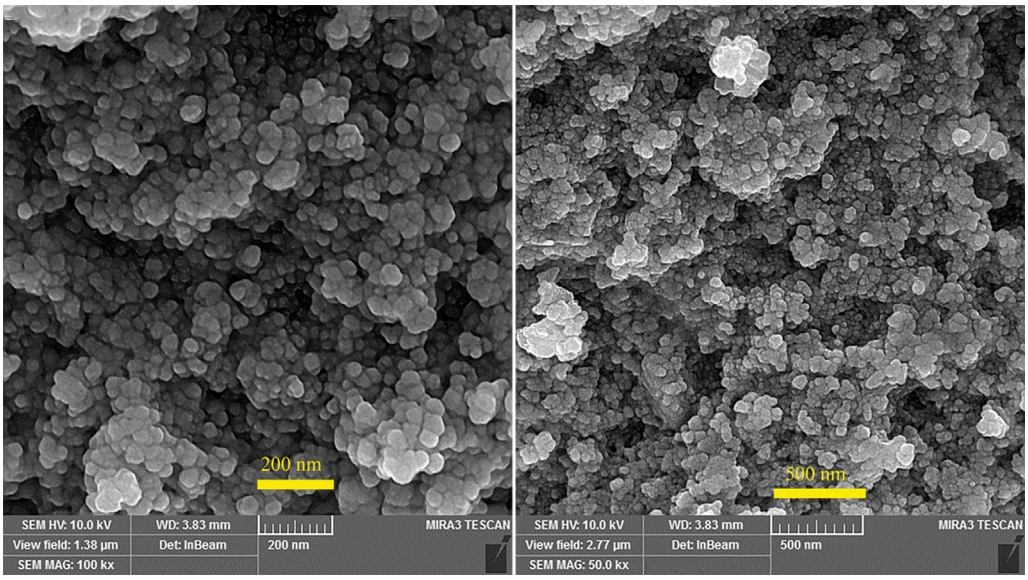

Fig. 4 Surface morphology of synthesized silver nanoparticle from the aerial extracts of *S. ebulus* by FESEM.

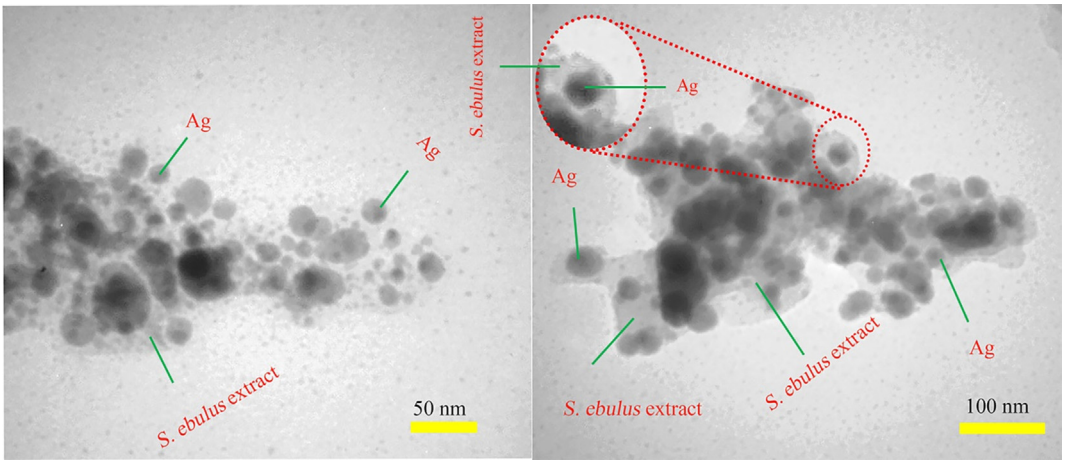

Fig. 5 TEM images of synthesized silver nanoparticles using *S. ebulus* extract (sample no. 10).

of *S. ebulus* extract and *S. ebulus*-capped AgNPs (sample no. 10). The FT-IR spectra of phytogenic AgNPs@*SEE* (sample no. 10) showed intense bands at 3348.19, 2929.67, 1623.95, 1401.65, 1273.12, and 1060.78 cm^{-1}. Generally, the FT-IR spectrum of AgNPs@*SEE* is similar to that of the *S. ebulus* extract, with a slight shift in the band positions (Patil et al., 2018). The FT-IR spectrum of sample no. 10 showed a broad and strong band at 3348.19 cm^{-1} that can be assigned to the O-H stretching band of alcohols or phenols. The O-H stretching vibration of the carboxylic acids was observed at 2929.67 cm^{-1}. The distinct peak located at 1623.95 cm^{-1} represents the symmetrical stretching vibration of –C = O group (Gomathi et al., 2017). Two absorption bands observed at 1401.65 and 1273.12 cm^{-1} are attributed to the –C-H bend of alkanes or –C-C- the stretch of aromatics and C-O bending vibration of anhydrides group, respectively (Rasheed et al., 2017).

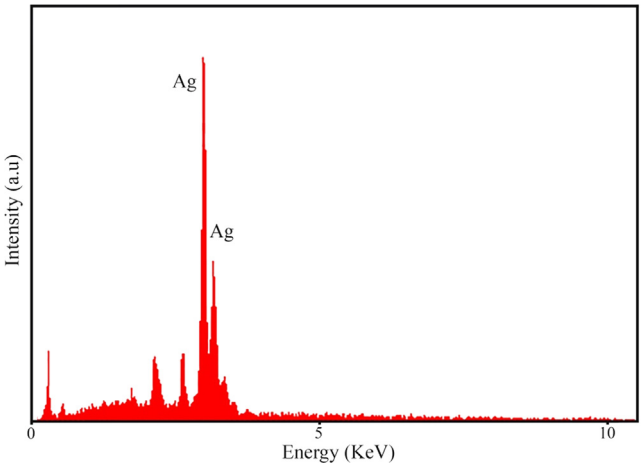

Fig. 6 EDS spectrum of AgNPs from *S. ebulus* extract.

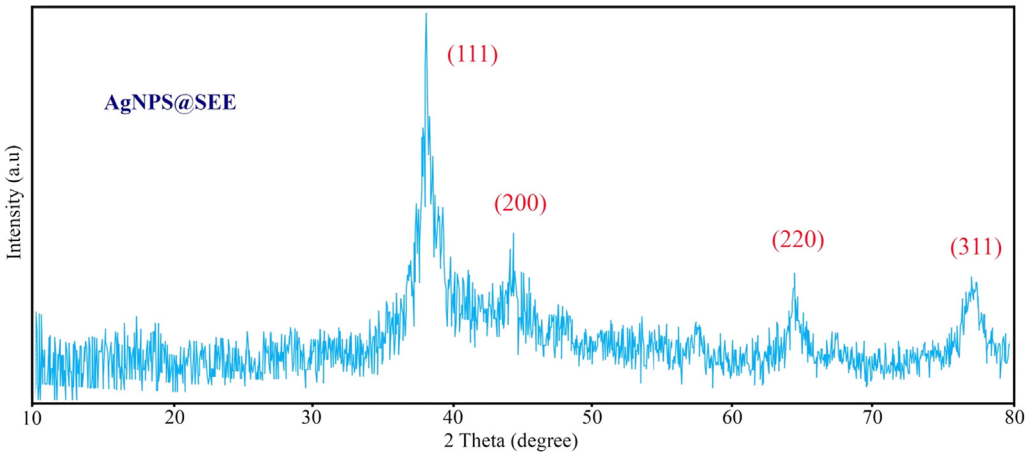

Fig. 7 XRD pattern of silver nanoparticles (sample no. 10).

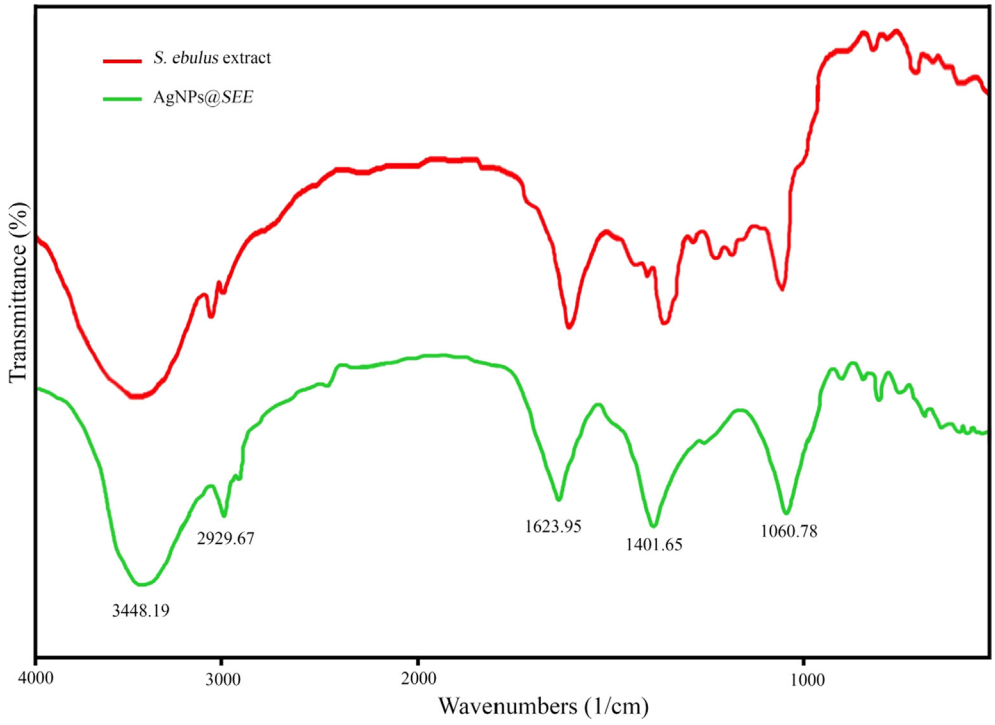

Fig. 8 FT-IR spectra of AgNPs@*SEE* (sample no. 10) and *S. ebulus* extract.

3.6. Dynamic light scattering analysis

Dynamic light scattering (DLS) and zeta-potential analysis were applied to determine the hydrodynamic size and surface charge of nanoparticles. The DLS diagram of synthesized silver nanoparticles in optimal conditions (sample no. 10) is shown in Fig. 9. The DLS results show that the average hydrodynamic size of the *S. ebulus*-capped silver nanoparticles was about 90–110 nm. The negative or positive charge on the surface of nanomaterials prevents aggregation of nanomaterials by same charges repulsion (Shirzadi-Ahodashti et al., 2021). The zeta potential value was determined to be −19.1 mV which indicated negative charges on the formed AgNPs@*SEE*.

3.7. Antibacterial evaluation

In this research, two series of ATCC bacteria and clinically isolated bacteria were chosen to examine their susceptibility against synthesized AgNPs@*SEE* (Table 4 and Table 5). The synthesized AgNPs (sample no. 10) in the presence of *S. ebulus* extract were analyzed for antibacterial property against two Gram positive bacteria like *E. faecalis*, *S.aureus* and five Gram negative bacteria like *E. coli, K. pneumoniae*, *P. mirabilis*, *P. aeruginosa,* and *A. baumannii*. The test pathogens were treated with several concentrations of AgNPs@SEE (1.5–400 µg/mL) and *S. ebulus* extract (4000 to 500 µg/ml). Then, the MIC assay of seven Gram-negative and positive bacterial was determined

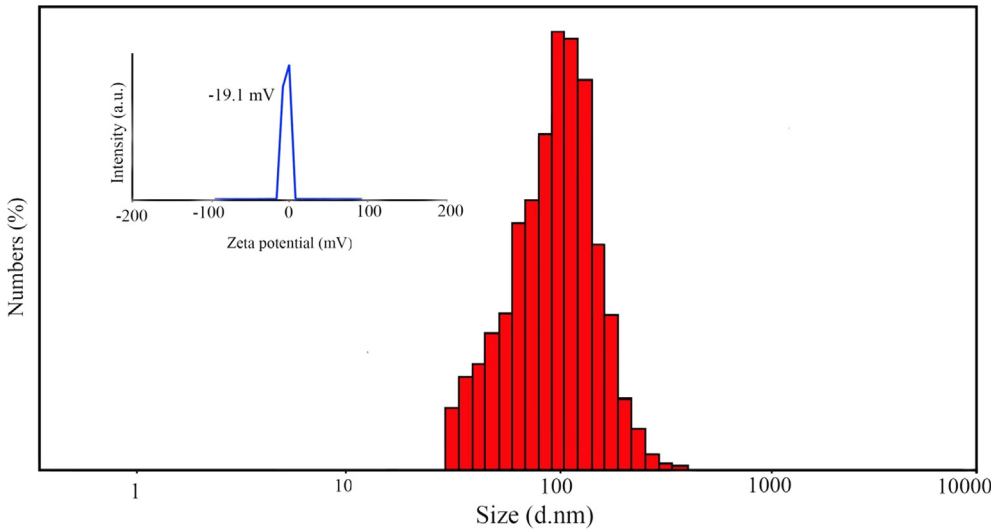

Fig. 9 DLS spectrum of silver nanoparticles at a concentration of 20 mM of silver nitrate salt (sample no. 10) at 4 h and 85 ℃.

Table 4 MIC and MBC values (μg/mM) for AgNPs@*SEE* tested using various bacterial strains.

Microorganism	MIC (μg/ml)	MBC (μg/ml)	Extract MIC (μg/ml)	Ciprofloxacin MIC (μg/ml)
S. aureus ATCC 29213	1.5	50	4000 <	0.21
E. faecalis ATCC 29212	50	200	4000 <	0.21
P. aeruginosa ATCC27853	6.25	200	4000 <	0.51
A. baumannii ATCC 19606	3.66	100	4000 <	0.25
E. coli ATCC 25922	3.66	50	4000 <	0.1
K. pneumoniae ATCC700603	3.66	100	4000 <	0.1
P. mirabili ATCC 25933	6.25	12.5	4000 <	0.1

Table 5 Resistance profile of clinical isolates and MIC, MBC of the synthesized AgNPs@*SEE* against various strains microorganism.

Bacteria	Treatment with NPs		Susceptibility to antimicrobial agents										
	MBC AgNPs (μg/ml)	MIC AgNPs (μg/ml)	MC	VC	OC	TC	GM	PC	CIF	CEZ	ERM	CM	AK
S. aureus	400	25	R	R	R	S	R	R	R	R	R	R	R
E. faecalis	400	100	S	R	R	R	R	R	S	R	R	R	R
P. aeruginosa	50	1.5	R	R	R	R	R	R	R	R	R	R	R
A. baumannii	100	3.125	R	R	R	R	R	R	R	R	R	R	R
E. coli	100	3.125	R	R	R	R	R	R	R	R	R	R	R
K. pneumoniae	200	50	R	R	R	R	R	R	R	R	R	R	R
P. mirabilis	100	6.25	R	R	R	R	R	R	R	R	R	R	R

R, resistant; **S**, susceptible**; MC**, Meticillin; **VC**, Vancomycin; **OC**, Oxacillin; **TC**, Tetracycline; **GM**, Gentamicin; **PC**, Penicillin; **CIF,** Ciprofloxacin; **CEZ**, Ceftazidime; **ERM**, Erythromycin; **CM**, Clindamycin; **AK**, Amikacin.

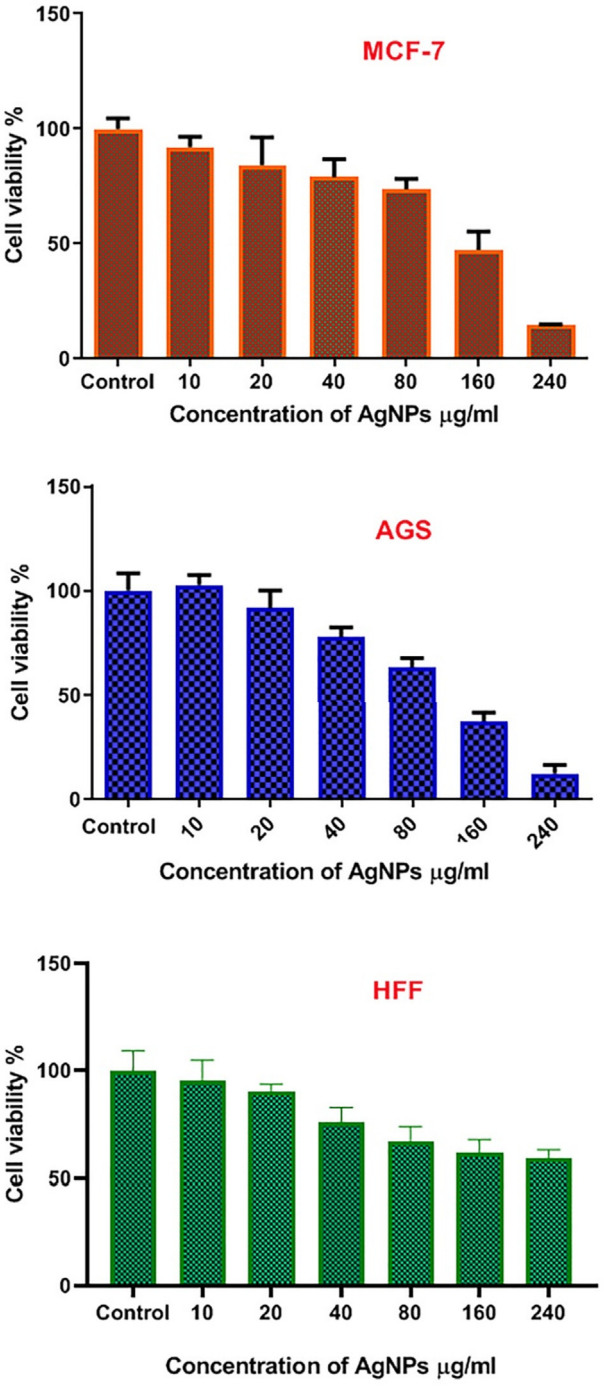

Fig. 10 Cytotoxicity assay of the synthesized AgNPs@*SEE* against: MCF-7, AGS and HFF cell lines.

for both ATCC and MDR strains by broth dilution method. The antibacterial activity of AgNPs@*SEE* showed that the MIC value of bacteria decreased with the increasing concentration of AgNPs@*SEE*. The MIC and MBC values in this research are listed in Table 4. As can be observed, *S. aureus* was found to be the most sensitive strain to the AgNPs@*SEE* (sample no. 10) with MIC and MBC values of 1.5 and 50 µg/ml, respectively. In contrast, *E. faecalis* showed the least sensitivity to the synthesized AgNPs@*SEE* with MIC and MBC values of 50 and 200 µg/ml, respectively. In recent years, different mechanisms of antibacterial activity were proposed including: release of lipopolysaccharides, electrostatic interaction, the involvement of free radicals, disturbance of membrane permeability and cell membrane (Dibrov et al., 2002; Kim et al., 2007). The exact antibacterial mechanism of action of silver nanoparticles has not yet been confirmed. But, our proposed mechanism of antibacterial activity can be described as follow (Shao et al., 2020): (i) destruction of the cell wall by binding and penetration of AgNPs@*SEE* into the cell membrane; (ii) reaction with the tiol groups of proteins; (iii) death of microorganism cells by prevention of DNA replication. In a comprehensive study on the clinical isolated bacteria, *K. pneumoniae* (positive for OXA-23, NMD and negative for VIM), *S. aureus* (the presence of the genes encoding the enzymes of the carbapenemase OXA-24 and OXA-23 is confirmed) with MIC values of 25 and 50 µg/ml and peripheral *E. faecalis* (positive for ermB, TetM, TetL, VanA, VanB) with MIC value of 100 µg/ml revealed moderate antibacterial activity (Table. 5). In this study the higher antibacterial activity observed for *A. baumannii* (with MIC value 3.25 µg/ml), *P. aeruginosa* (with MIC value 1.5 µg/ml), which was isolated from wound and phlegm. The MIC value of *P. mirabilis* (positive for OXA-23 and negative for NMD, VIM, PhosA3) and *E. coli* (positive for OXA-23, PhosA3 and VIM and negative for NMD) were 6.25 and 3.125 µg/ml, respectively.

3.8. Cytotoxicity evaluation

Anti-cancer activity of synthesized AgNPs@*SEE* (sample no. 10) was assessed against breast (MCF-7) and gastric (AGS) cancer cell lines with fibroblast as normal cells (HFF). The synthesized silver nanoparticles displayed weak growth inhibition against HFF cells, even at high concentration (240 µg/ml). The synthesized silver nanoparticles displayed weak growth inhibition against HFF cells, even at high concentration (240 µg/ml, IC_{50}: 58.54 µg/ml). In vitro cytotoxicity of synthesized AgNPs@*SEE* (sample no. 10) was determined against cancer cell lines (MCF-7 and AGS) at various concentrations (10–240 µg/ml). The results showed (Fig. 10) that the cancer cell death increased with increasing concentrations of AgNPs@*SEE*. Metallic silver nanoparticles (sample no. 10) had potential to inhibit the growth of MCF-7 cell line around 13% at low concentration (10 µg/ml, IC_{50}: 62.37 µg/ml). On the other hand, the presence of 240 µg/ml of AgNPs@*SEE* (sample no. 10) meaningfully inhibited the cell growth over 85%. The same results observed for AGS cell line, cell viability determination was revealed that the percentage of the live cells decreased with increasing the concentration of synthesized AgNPs. Synthesized AgNPs could inhibit the growth of the AGS cell line around 1% at a low concentration (10 mg/ml, IC_{50}: 67.87 µg/ml). In contrast, the presence of 240 µg/ml of synthesized AgNPS significantly inhibited cell growth over 90%. Cell death occurred by AgNPs@*SEE* (sample no 10) with inducing reactive oxygen species and cause damage to cellular components. Sabinene, terpinen, carvacrol, linalool, thymol, quercetin, apigenin, terpinolene and rutin as bioactive compounds in the biosynthesis of AgNPs@*SEE* are responsible for making better cytotoxic effects.

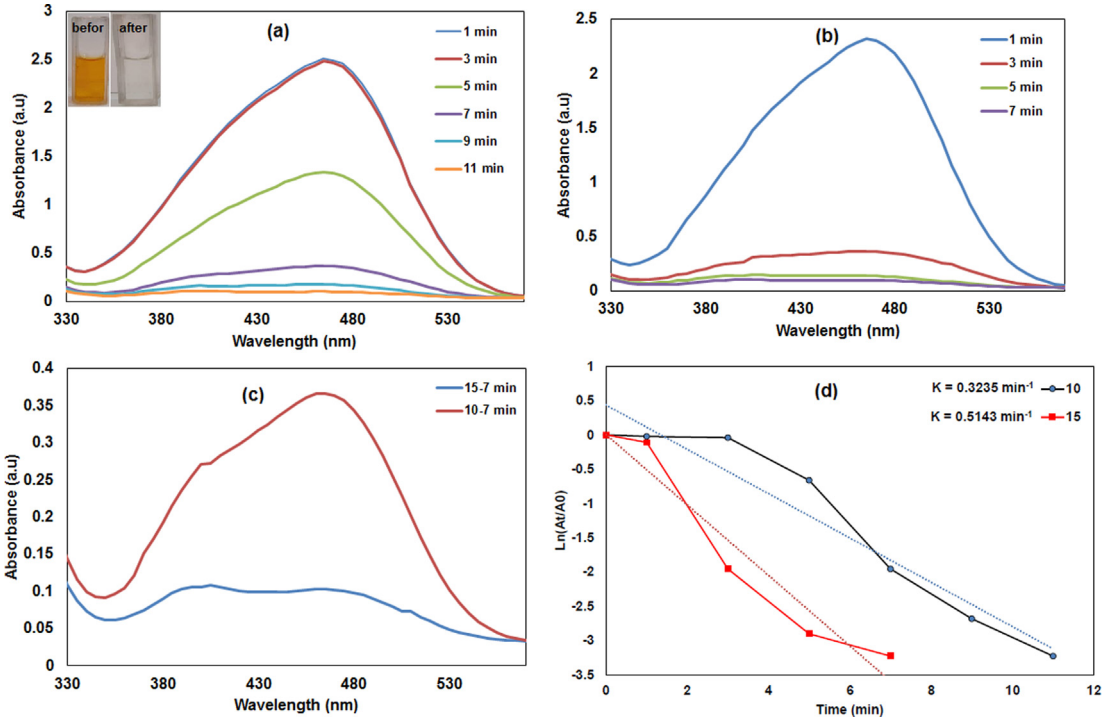

Fig. 11 UV–Vis absorption spectra of reduction of MO in the presence of $NaBH_4$ and AgNPs as catalyst at a) 10 µl AgNPs; b) 15 µl AgNPs; c) Comparison of 10 and 15 µl AgNPs and d) degradation kinetics of MO.

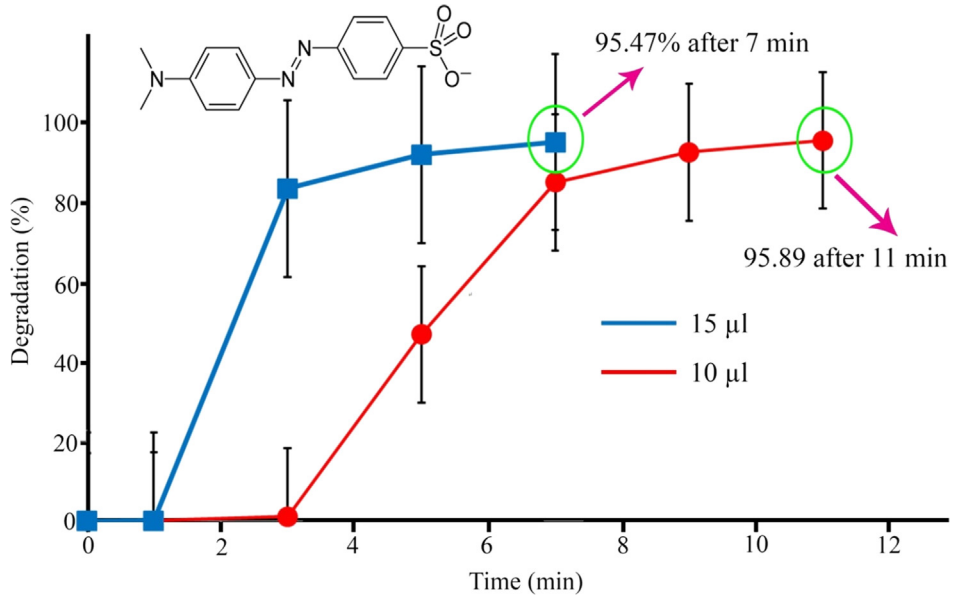

Fig. 12 Photocatalytic degradation of MO hazardous pollutant under sun-light irradiation.

3.9. Photocatalytic activity

The catalytic performance of synthesized AgNPs@*SEE* was investigated with the degradation of methyl orange (MO) through $NaBH_4$. In the absence of AgNPs, the reducing power of $NaBH_4$ is weak (blank test). The degradation of MO occurred by adding different volumes of prepared AgNPs into the mixture of $NaBH_4$ and MO solution and the absorption intensity of MO decreased at 470 nm. The orange color of MO as an azo dye was reduced to colorless hydrazine derivatives that were confirmed in Fig. 11. Volumes 10 and 15 µl of synthesized AgNPs, completely degraded MO in 11 and 7 min, respectively (Fig. 11a-c) that the rate of dye degradation was followed using UV–Vis spectra. The peak intensity obtained from the degradation reaction at 470 nm gradually reduced and the rate constants were obtained 0.3235 min^{-1} and

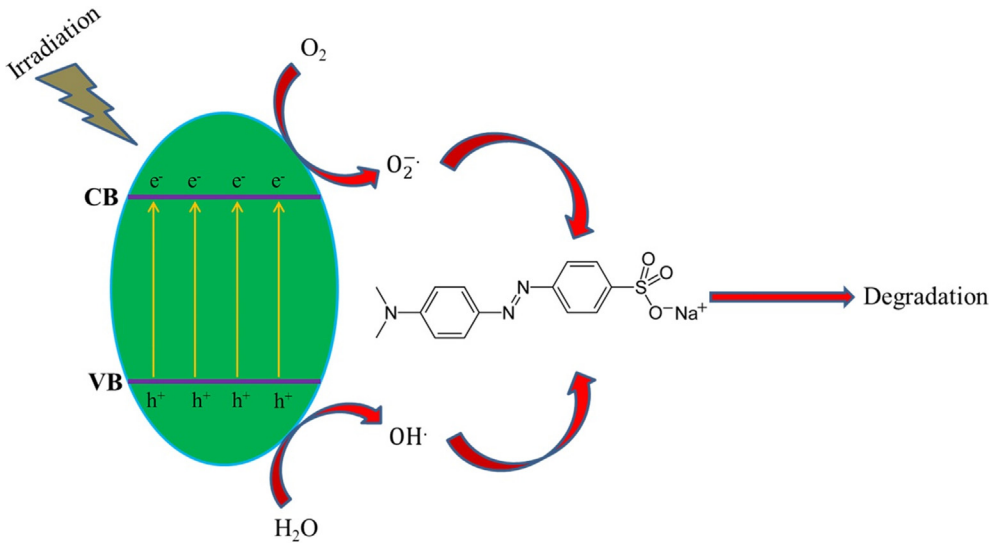

Fig. 13 Probable degradation mechanism of pollutants by AgNPs@*SEE* under sun-light irradiations.

0.5143 min^{-1}, respectively (Fig. 11c, d). This is due to the increase in the surface area of the active site of Ag nanocatalyst as AgNPs content increases. Consequently, the rate of the reaction was increased slowly. This revealed that the AgNPs mediated the extract showed good photocatalytic activity in the degradation of MO as a dye contaminant. Also, Fig. 12 displays the percentage of dye degradation at different times. The overall reaction during photocatalysis with sun-light is shown below (Fig. 13):

$$AgNPs + hv \rightarrow AgNPs(e^{-}_{CB} + h^{+}_{VB}) \quad (4)$$

$$\mathrm{AgNPs(huv)} + H_2O \rightarrow \mathrm{Ag0} + H^{\cdot} + OH^{\cdot} \quad (5)$$

$$O_2^{-\cdot} + \mathrm{H+} \rightarrow HO_2^{\cdot} \quad (6)$$

$$\mathrm{Dye} + OH^{\cdot} \rightarrow \mathrm{degradationproducts} \quad (7)$$

$$\mathrm{Dye} + h^{+}_{VB} \rightarrow \mathrm{oxidationproducts} \quad (8)$$

$$\mathrm{Dye} + e^{-}_{CB} \rightarrow \mathrm{reductionproducts} \quad (9)$$

4. Conclusion

In the current study AgNPs@*SEE* was successfully synthesized using *S. ebulus* extract as stabilizing, capping and reducing agents. From TEM and FESEM images, it is confirmed that the AgNPs@*SEE* produced were spherical in morphology with size ranges about 35–50 nm. The biosynthesized AgNPs@*SEE* had effective anti-cancer effects against breast (MCF-7) and gastric (AGS) cancer cell lines. The biogenic *AgNPs@SEE* was used as a nanocatalyst, which showed high catalytic activity for degradation of methyl orange under sun-light irradiation. Furthermore, biosynthesized silver nanoparticles revealed high antibacterial activity against Gram-positive and Gram-negative bacteria. The *AgNPs@SEE* displayed the highest activity against *S. aureus*, *A. baumannii*, *E. coli*, and *K. pneumoniae* among the various bacterial strains tested. It appears that the silver nanoparticles synthesized using *S. ebulus* extract can be applied as novel anti-cancer, antibacterial, and catalytic agents in the near future.

Declaration of Competing Interest

The authors declare that they have no known competing financial interests or personal relationships that could have appeared to influence the work reported in this paper.

Acknowledgment

Research reported in this publication was supported by Elite Researcher Grant Committee under award number [958433] from the National Institutes for Medical Research Development (NIMAD), Tehran, Iran.

References

Mohammadzadeh, P., Shafiee Ardestani, M., Mortazavi-Derazkola, S., Bitarafan-Rajabi, A., Ghoreishi, S.M., 2019. PEG-Citrate dendrimer second generation: is this a good carrier for imaging agents In Vitro and In Vivo? IET Nanobiotechnol. 13, 560–564.

Ghoreishi, S.M., Khalaj, A., Bitarafan-Rajabi, A., Azar, A.D., Ardestani, M.S., Assadi, A., 2017. Novel 99mTc-Radiolabeled Anionic Linear Globular PEG-Based Dendrimer-Chlorambucil: Non-Invasive Method for In-Vivo Biodistribution. Drug Res. 67, 149–155.

Mohammadi-Aghdam, S., Valinezhad-Saghezi, B., Mortazavi, Y., Qhoreishi, S.M., 2018. Modified Fe_3O_4/HAP magnetically nanoparticles as the carrier for ibuprofen: Adsorption and release study. Drug Res. 69, 93–99.

Ardestani, M.S., Bitarafan-Rajabi, A., Mohammadzadeh, P., Mortazavi-Derazkola, S., Sabzevari, O., Azar, A.D., Kazemi, S., Hosseini, S.R., Ghoreishi, S.M., 2020. Synthesis and characterization of novel 99mTc-DGC nano-complexes for improvement of heart diagnostic. Bioorg. Chem. 96.

Ebrahimzadeh, M.A., Naghizadeh, A., Mohammadi-Aghdam, S., Khojasteh, H., Ghoreishi, S.M., Mortazavi-Derazkola, S., 2020. Enhanced catalytic and antibacterial efficiency of biosynthesized Convolvulus fruticosus extract capped gold nanoparticles (CFE@AuNPs). J. Photochem. Photobiol., B 209, 111949.

Kumari, P., Meena, A., 2020. Green synthesis of gold nanoparticles from Lawsoniainermis and its catalytic activities following the Langmuir-Hinshelwood mechanism. Colloids Surf., A 606, 125447.

Yugay, Y.A., Usoltseva, R.V., Silant'ev, V.E., Egorova, A.E., Karabtsov, A.A., Kumeiko, V.V., Ermakova, S.P., Bulgakov, V. P., Shkryl, Y.N., 2020. Synthesis of bioactive silver nanoparticles using alginate, fucoidan and laminaran from brown algae as a reducing and stabilizing agent. Carbohydr. Polym. 245, 116547.

Rabiee, N., Bagherzadeh, M., Kiani, M., Ghadiri, A.M., 2020. Rosmarinus officinalis directed palladium nanoparticle synthesis: Investigation of potential anti-bacterial, anti-fungal and Mizoroki-Heck catalytic activities. Adv. Powder Technol. 31, 1402–1411.

Yarahmadi, M., Maleki-Ghaleh, H., Mehr, M.E., Dargahi, Z., Rasouli, F., Siadati, M.H., 2021. Synthesis and characterization of Sr-doped ZnO nanoparticles for photocatalytic applications. J. Alloy. Compd. 853, 157000.

Pushpamalini, T., Keerthana, M., Sangavi, R., Nagaraj, A., Kamaraj, P., 2021. Comparative analysis of green synthesis of TiO2 nanoparticles using four different leaf extract. Mater. Today:. Proc. 40, S180–S184.

Mali, S.C., Dhaka, A., Githala, C.K., Trivedi, R., 2020. Green synthesis of copper nanoparticles using Celastrus paniculatus Willd. leaf extract and their photocatalytic and antifungal properties. Biotechnol. Rep, 27, e00518.

Mortazavi-Derazkola, S., Ebrahimzadeh, M.A., Amiri, O., Goli, H.R., Rafiei, A., Kardan, M., Salavati-Niasari, M., 2020. Facile green synthesis and characterization of Crataegus microphylla extract-capped silver nanoparticles (CME@Ag-NPs) and its potential antibacterial and anticancer activities against AGS and MCF-7 human cancer cells. J. Alloy. Compd. 820, 153186.

Yousaf, H., Mehmood, A., Ahmad, K.S., Raffi, M., 2020. Green synthesis of silver nanoparticles and their applications as an alternative antibacterial and antioxidant agents. Mater. Sci. Eng., C 112, 110901.

Ebrahimzadeh, M.A., Naghizadeh, A., Amiri, O., Shirzadi-Ahodashti, M., Mortazavi-Derazkola, S., 2020. Green and facile synthesis of Ag nanoparticles using Crataegus pentagyna fruit extract (CP-AgNPs) for organic pollution dyes degradation and antibacterial application. Bioorg. Chem. 94, 103425.

Uluturhan, E., Kucuksezgin, F., 2007. Heavy metal contaminants in Red Pandora (Pagellus erythrinus) tissues from the Eastern Aegean Sea, Turkey. Water Res. 41, 1185–1192.

Anjana, V.N., Koshy, E.P., Mathew, B., 2020. Facile synthesis of silver nanoparticles using Azolla caroliniana, their cytotoxicity, catalytic, optical and antibacterial activity. Mater. Today:. Proc. 25, 163–168.

Sangaonkar, G.M., Pawar, K.D., 2018. Garcinia indica mediated biogenic synthesis of silver nanoparticles with antibacterial and antioxidant activities. Colloids Surf., B 164, 210–217.

Rolim, W.R., Pelegrino, M.T., de Araújo Lima, B., Ferraz, L.S., Costa, F.N., Bernardes, J.S., Rodigues, T., Brocchi, M., Seabra, A. B., 2019. Green tea extract mediated biogenic synthesis of silver nanoparticles: Characterization, cytotoxicity evaluation and antibacterial activity. Appl. Surf. Sci. 463, 66–74.

Ravichandran, A., Subramanian, P., Manoharan, V., Muthu, T., Periyannan, R., Thangapandi, M., Ponnuchamy, K., Pandi, B., Marimuthu, P.N., 2018. Phyto-mediated synthesis of silver nanoparticles using fucoidan isolated from Spatoglossum asperum and assessment of antibacterial activities, Journal of photochemistry and photobiology. B, Biology 185, 117–125.

Ravichandran, V., Vasanthi, S., Shalini, S., Shah, S.A.A., Tripathy, M., Paliwal, N., 2019. Green synthesis, characterization, antibacterial, antioxidant and photocatalytic activity of Parkia speciosa leaves extract mediated silver nanoparticles. Results Phys. 15, 102565.

Shokrzadeh, M., Saeedi Saravi, S.S., 2010. The chemistry, pharmacology and clinical properties of Sambucus ebulus: A review. J. Med. Plants Res. 4, 095–103.

Ebrahimzadeh, M.A., Mahmoudi, M., Salimi, E., 2006. Antiinflammatory activity of Sambucus ebulus hexane extracts. Fitoterapia 77, 146–148.

Gutés, A., Céspedes, F., Alegret, S., del Valle, M., 2005. Determination of phenolic compounds by a polyphenol oxidase amperometric biosensor and artificial neural network analysis. Biosens. Bioelectron. 20, 1668–1673.

Notsu, H., Tatsuma, T., 2004. Simultaneous determination of phenolic compounds by using a dual enzyme electrodes system. J. Electroanal. Chem. 566, 379–384.

Shirzadi-Ahodashti, M., Mizwari, Z.M., Hashemi, Z., Rajabalipour, S., Ghoreishi, S.M., Mortazavi-Derazkola, S., Ebrahimzadeh, M. A., 2021. Discovery of high antibacterial and catalytic activities of biosynthesized silver nanoparticles using C. fruticosus (CF-AgNPs) against multi-drug resistant clinical strains and hazardous pollutants. Environ. Technol. Innovation 23.

Naghizadeh, A., Mizwari, Z.M., Ghoreishi, S.M., Lashgari, S., Mortazavi-Derazkola, S., Rezaie, B., 2021. Biogenic and eco-benign synthesis of silver nanoparticles using jujube core extract and its performance in catalytic and pharmaceutical applications: Removal of industrial contaminants and in-vitro antibacterial and anticancer activities. Environ. Technol. Innovation 23.

Shirzadi-Ahodashti, M., Ebrahimzadeh, M.A., Ghoreishi, S.M., Naghizadeh, A., Mortazavi-Derazkola, S., 2020. Facile and eco-benign synthesis of a novel $MnFe_2O_4$@SiO_2@Au magnetic nanocomposite with antibacterial properties and enhanced photocatalytic activity under UV and visible-light irradiations. Appl. Organomet. Chem. 34.

Celiktas, O.Y., Kocabas, E.E.H., Bedir, E., Sukan, F.V., Ozek, T., Baser, K.H.C., 2007. Antimicrobial activities of methanol extracts and essential oils of Rosmarinus officinalis, depending on location and seasonal variations. Food Chem. 100, 553–559.

Ebrahimzadeh, M.A., Hashemi, Z., Mohammadyan, M., Fakhar, M., Mortazavi-Derazkola, S., 2021. In vitro cytotoxicity against human cancer cell lines (MCF-7 and AGS), antileishmanial and antibacterial activities of green synthesized silver nanoparticles using Scrophularia striata extract. Surf. Interfaces 23.

Pereira, T.M., Polez, V.L.P., Sousa, M.H., Silva, L.P., 2020. Modulating physical, chemical, and biological properties of silver nanoparticles obtained by green synthesis using different parts of the tree Handroanthus heptaphyllus (Vell.) Mattos, Colloid and Interface Science. Communications 34, 100224.

Patil, M.P., Kim, G.-D., 2017. Eco-friendly approach for nanoparticles synthesis and mechanism behind antibacterial activity of silver and anticancer activity of gold nanoparticles. Appl. Microbiol. Biotechnol. 101, 79–92.

Maity, G.N., Maity, P., Choudhuri, I., Sahoo, G.C., Maity, N., Ghosh, K., Bhattacharyya, N., Dalai, S., Mondal, S., 2020. Green synthesis, characterization, antimicrobial and cytotoxic effect of silver nanoparticles using arabinoxylan isolated from Kalmegh. Int. J. Biol. Macromol. 162, 1025–1034.

Oliveira, G.Z.S., Lopes, C.A.P., Sousa, M.H., Silva, L.P., 2019. Synthesis of silver nanoparticles using aqueous extracts of Pterodon emarginatus leaves collected in the summer and winter seasons, International. Nano Lett. 9, 109–117.

Shirzadi-Ahodashti, M., Mortazavi-Derazkola, S., Ebrahimzadeh, M. A., 2020. Biosynthesis of noble metal nanoparticles using crataegus monogyna leaf extract (CML@X-NPs, X = Ag, Au): Antibacterial and cytotoxic activities against breast and gastric cancer cell lines. Surf. Interfaces 21.

Jyoti, K., Baunthiyal, M., Singh, A., 2016. Characterization of silver nanoparticles synthesized using Urtica dioica Linn. leaves and their synergistic effects with antibiotics. J. Radiat. Res. Appl. Sci. 9, 217–227.

Patil, M.P., Singh, R.D., Koli, P.B., Patil, K.T., Jagdale, B.S., Tipare, A.R., Kim, G.D., 2018. Antibacterial potential of silver nanoparticles synthesized using Madhuca longifolia flower extract as a green resource. Microb. Pathog. 121, 184–189.

Gomathi, M., Rajkumar, P.V., Prakasam, A., Ravichandran, K., 2017. Green synthesis of silver nanoparticles using Datura stramonium leaf extract and assessment of their antibacterial activity. Resour.-Effic. Technol. 3, 280–284.

Rasheed, T., Bilal, M., Iqbal, H.M.N., Li, C., 2017. Green biosynthesis of silver nanoparticles using leaves extract of Artemisia vulgaris and their potential biomedical applications, Colloids and surfaces. B, Biointerfaces 158, 408–415.

Dibrov, P., Dzioba, J., Gosink, K.K., Häse, C.C., 2002. Chemiosmotic mechanism of antimicrobial activity of Ag(+) in Vibrio cholerae. Antimicrob Agents Chemother 46, 2668–2670.

Kim, J.S., Kuk, E., Yu, K.N., Kim, J.-H., Park, S.J., Lee, H.J., Kim, S.H., Park, Y.K., Park, Y.H., Hwang, C.-Y., Kim, Y.-K., Lee, Y.-S., Jeong, D.H., Cho, M.-H., 2007. Antimicrobial effects of silver nanoparticles, Nanomedicine: Nanotechnology. Biology and Medicine 3, 95–101.

Shao, Y., Zeng, R.-C., Li, S.-Q., Cui, L.-Y., Zou, Y.-H., Guan, S.-K., Zheng, Y.-F., 2020. Advance in Antibacterial Magnesium Alloys and Surface Coatings on Magnesium Alloys: A Review. Acta Metallurgica Sinica (English Letters) 33, 615–629.

Alsubki, R., Tabassum, H., Abudawood, M., Rabaan, A.A., Alsobaie, S.F., Ansar, S., 2021. Green synthesis, characterization, enhanced functionality and biological evaluation of silver nanoparticles based on Coriander sativum. Saudi J. Biol. Sci. 28, 2102–2108.

Kaplan, Ö., Gökşen Tosun, N., Özgür, A., Erden Tayhan, S., Bilgin, S., Türkekul, İ., Gökce, İ., 2021. Microwave-assisted green synthesis of silver nanoparticles using crude extracts of Boletus edulis and Coriolus versicolor: Characterization, anticancer, antimicrobial and wound healing activities. J. Drug Delivery Sci. Technol. 64, 102641.

Nouri, A., Tavakkoli Yaraki, M., Lajevardi, A., Rezaei, Z., Ghorbanpour, M., Tanzifi, M., 2020. Ultrasonic-assisted green synthesis of silver nanoparticles using Mentha aquatica leaf extract for enhanced antibacterial properties and catalytic activity, Colloid and Interface Science. Communications 35, 100252.

Awad, M.A., Hendi, A.A., Ortashi, K.M., Alzahrani, B., Soliman, D., Alanazi, A., Alenazi, W., Taha, R.M., Ramadan, R., El-Tohamy, M., AlMasoud, N., Alomar, T.S., 2021. Biogenic synthesis of silver nanoparticles using Trigonella foenum-graecum seed extract: Characterization, photocatalytic and antibacterial activities. Sens. Actuators, A 323, 112670.

Sharma, R., 2021. Synthesis of Terminalia bellirica fruit extract mediated silver nanoparticles and application in photocatalytic degradation of wastewater from textile industries. Mater. Today:. Proc. 44, 1995–1998.

Ezhilarasi, A.A., Vijaya, J.J., Kaviyarasu, K., Zhang, X., Kennedy, L. J., 2020. Green synthesis of nickel oxide nanoparticles using Solanum trilobatum extract for cytotoxicity, antibacterial and photocatalytic studies. Surf. Interfaces 20, 100553.

Anwar, Y., Alghamdi, K.M., 2020. Imparting antibacterial, antifungal and catalytic properties to cotton cloth surface via green route. Polym. Test. 81, 106258.

Gomathi, E., Jayapriya, M., Arulmozhi, M., 2021. Environmental benign synthesis of tin oxide (SnO2) nanoparticles using Actinidia deliciosa (Kiwi) peel extract with enhanced catalytic properties. Inorg. Chem. Commun. 130, 108670.